

A spline-regularized minimal residual algorithm for iterative attenuation correction in SPECT

M Péligrini†, I Buvat†‡, H Benali†, G El Fakhri†§, P Grangeat|| and R Di Paola†

† INSERM U494, CHU Pitié-Salpêtrière, 91 Boulevard de l'Hôpital, 75634 Paris Cedex 13, France

|| CEA/LETI Département Systèmes, 17 Rue des Martyrs, 38054 Grenoble Cedex 9, France

E-mail: buvat@imed.jussieu.fr

Received 16 September 1998, in final form 21 July 1999

Abstract. In SPECT, regularization is necessary to avoid divergence of the iterative algorithms used for non-uniform attenuation compensation. In this paper, we propose a spline-based regularization method for the minimal residual algorithm. First, the acquisition noise is filtered using a statistical model involving spline smoothing so that the filtered projections belong to a Sobolev space with specific continuity and derivability properties. Then, during the iterative reconstruction procedure, the continuity of the inverse Radon transform between Sobolev spaces is used to design a spline-regularized filtered backprojection method, by which the known regularity properties of the projections determine those of the corresponding reconstructed slices. This ensures that the activity distributions estimated at each iteration present regularity properties, which avoids computational noise amplification, thus stabilizing the iterative process. Analytical and Monte Carlo simulations are used to show that the proposed spline-regularized minimal residual algorithm converges to a satisfactory stable solution in terms of restored activity and homogeneity, using at most 25 iterations, whereas the non regularized version of the algorithm diverges. Choosing the number of iterations is therefore no longer a critical issue for this reconstruction procedure.

1. Introduction

In SPECT, attenuation correction is necessary to achieve reliable quantitative measurements from the reconstructed activity distributions. Many correction methods have been proposed (King *et al* 1996) which can be divided into analytical and iterative approaches. Analytical corrections (e.g. Bellini *et al* 1979, Tretiak and Metz 1980) provide an exact solution to the inversion of the attenuated Radon transform for a uniform attenuating medium with a convex support. However, the assumption of a uniform attenuating medium limits their clinical applications. For non-uniform attenuating media (e.g. in cardiac imaging), there are no analytical solutions to the inversion of the attenuated Radon transform and iterative approaches are preferred. Iterative methods based on filtered backprojection (FBP) reconstruction (e.g. Chang 1978) use only few iterations, typically less than five (Murase *et al* 1987), because their sensitivity to noise make them diverge rapidly. Expectation-maximization (EM) and gradient reconstruction methods can also be used for attenuation correction by modelling attenuation

‡ To whom correspondence should be addressed.

§ Present address: Harvard Medical School, Boston, MA, USA.

in the projector/backprojector pair. The theoretical convergence of these algorithms in the absence of noise has been demonstrated but many iterations are needed, typically more than 50 for ML-EM algorithms. In that regard, the conjugate gradient (CG) has proven to converge five times faster than ML-EM algorithms (Zhao *et al* 1994). Ordered subsets used in iterative algorithms can also accelerate the convergence (Hudson and Larkin 1994). However, both gradient and EM methods remain sensitive to noise as the number of iterations increases, thus requiring a regularization procedure (Kawata and Nalcioglu 1985, Green 1990). Iterative methods are sensitive not only to the measurement noise affecting the acquired projections, but also to computational noise arising from the ill-posed nature of the reconstruction procedure as the number of iterations increases.

In this paper, we focus on the minimal residual (MR) algorithm, which is a gradient-type algorithm using an asymmetric projector/backprojector pair (i.e. the attenuation is modelled in the projector and not in the backprojector). Unlike the CG algorithm, the MR algorithm does not necessarily converge to a global minimum solution (Axelsson 1980, Greenbaum 1997), yet it has been shown to give similar results to those obtained with CG for attenuation correction in SPECT, using four times fewer iterations (La *et al* 1996, La and Grangeat 1998). MR presents about the same sensitivity to noise as CG (e.g. Kawata and Nalcioglu 1985, La *et al* 1996, La and Grangeat 1998) and therefore also needs to be regularized to avoid divergence. Regularization of gradient-type algorithms (CG, MR) has already been proposed using spatial constraints related to the reconstructed activity distributions (Kawata and Nalcioglu 1985, La *et al* 1996, La and Grangeat 1998) or probability constraints (Lalush and Tsui 1995).

In this paper, we propose a spline-based regularization approach for the MR algorithm, the spline-regularized minimal residual (SRMR) method. SRMR extends the regularized backprojection method that we previously designed to address the ill-posed nature of tomographic reconstruction (Péligrini *et al* 1998) to an iterative reconstruction procedure accounting for non-uniform attenuation. As in our previous work, we first derive a statistical model which reduces the acquisition noise and ensures that the resulting filtered projections belong to a known Sobolev space. A Sobolev space is a space of functions having specific properties of continuity and derivability, which we term 'regularity properties'. Our novel contribution here consists in modifying the conventional MR iterative algorithm by constraining the activity distributions estimated at each iteration to belong to another Sobolev space, whose characteristics are deduced from those of the Sobolev space containing the filtered projections. This approach reduces the computation noise as the number of iterations increases, stabilizes the iterative procedure and guarantees a regularized attenuation-corrected activity distribution.

Section 2 describes the MR algorithm. Section 3 presents the SRMR method. Sections 4 and 5 illustrate the method using analytical and Monte Carlo simulations. The value of the method is discussed in section 6.

2. The minimal residual algorithm

In SPECT attenuation correction, the minimal residual algorithm (Axelsson 1980) is used for solving the following inverse problem (La *et al* 1996, La and Grangeat 1998):

$$R^* R_\mu f = R^* p \quad (1)$$

where p represents the acquired SPECT projections, f is the unknown activity distribution, R_μ is an attenuated projection operator and R^* is an operator that may be regarded as a preconditioning operator, since it improves the condition number of the system, hence the

Table 1. MR algorithm.

Initialization	$r^0 = R^*p - Af^0, d^0 = r^0, t^0 = Ad^0$
Step n	$\alpha^n = \frac{\langle r^n, t^n \rangle}{\ t^n\ ^2}$ $f^{n+1} = f^n + \alpha^n d^n$ $r^{n+1} = r^n - \alpha^n t^n$ $\beta^{n+1} = -\frac{\langle Ar^{n+1}, t^n \rangle}{\ t^n\ ^2}$ $d^{n+1} = r^{n+1} + \beta^{n+1} d^n$ $t^{n+1} = Ar^{n+1} + \beta^{n+1} t^n$

$\langle x, y \rangle = x^t y$ denotes the scalar product of vectors x and y .

convergence rate of the algorithm. The algorithm is called ‘minimal residual’ because it reduces the squared residual error $\|R^*R_\mu f - R^*p\|^2$ at each iteration. R^* should be chosen as close to R_μ^{-1} as possible so that $A = R^*R_\mu$ is close to the identity matrix, which ensures that the MR algorithm converges monotonically to a minimum (Axelsson 1980, Greenbaum 1997, La and Grangeat 1998). An example of operator R^* is the filtered backprojection operator (Walters *et al* 1981, La *et al* 1996, La and Grangeat 1998). When A is a symmetric positive definite matrix, MR converges to a unique solution and the inverse problem is solved using conventional conjugate gradient algorithms. MR can therefore be viewed as a generalization of CG algorithms to asymmetric A operators.

If f^0 is the initial activity distribution estimate, the MR algorithm is given in table 1. f^{n+1} is the activity distribution estimate at step $n \geq 0$, α^n is the step size in the search direction d^n and $r^n = R^*p - Af^n$ is the residual vector. β^n and $t^n = Ad^n$ are additional convenient parameters of the MR algorithm.

3. The spline-regularized minimal residual algorithm (SRMR)

Our approach takes advantage of the fact that the projections *and* the corresponding activity distributions are intrinsically continuous. We model this continuity by assuming that projections *and* activity distributions belong to spaces of functions having specific properties of derivability and continuity. More specifically, we consider Sobolev spaces of order $\alpha \in \mathbb{R}$ (Adams 1975), denoted by $H^{(\alpha)}$ (see appendix A for a definition). For m an integer, $H^{(m)}$ is simply the space of functions having absolutely continuous derivatives up to order $m - 1$, and such that the square of their m th derivative has a finite integral. For convenience sake, we term ‘regularity properties’ the properties of continuity and derivability of functions belonging to a given Sobolev space.

To deal with the properties of Sobolev spaces, SRMR includes two steps (figure 1): regularization of the projections by noise filtering and regularization of the iterative reconstruction procedure. The measurement noise in the projections is first reduced so that the resulting filtered projections belong to a specific Sobolev space (section 3.1). Then, the operator R^* used for the iterative reconstruction is chosen so that it constrains the estimated activity distribution to also belong to a specific Sobolev space which is consistent with the Sobolev space the filtered projections belong to (section 3.2). The activity distributions estimated at each iteration therefore present specific regularity properties, which ensures the regularization of the iterative process.

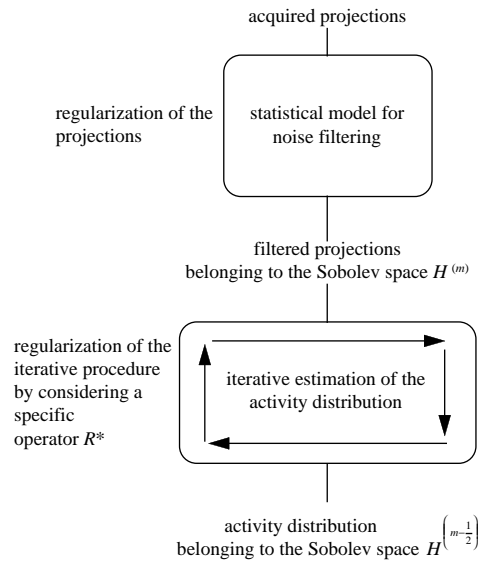


Figure 1. Spline-regularized minimal residual (SRMR) algorithm: summary of the processing steps.

3.1. Noise filtering

The statistical model presented in Péligrini *et al* (1998) to filter the acquisition noise in the sinograms has been generalized so that all sinograms are filtered simultaneously instead of processing each slice independently. Using this model, reduced-noise projections belonging to a specific Sobolev space are estimated.

3.1.1. Statistical model for noise filtering. Let p denote the acquired discrete projections, consisting of N projection angles, K projection bins and S slices. The K -vector p_{ij} represents the variation of the signal along the direction of the bins within the slice j ($j = 1, S$) of the projection i ($i = 1, N$).

Let us assume that one can define a continuous transform T so that the process underlying the transformed projections $p' = T(p)$ presents a variance which is stationary in space (i.e. which does not depend on the projection bin k).

If there were no noise, the acquired projections p'_{ijk} ($k = 1, K$) should be the discretization of projections p' which are *continuous* along the direction of the projections bins because of the finite spatial response function of the acquisition device. This intrinsic regularity of the continuous projections p' can be modelled by assuming that p' belongs to a Sobolev space $H^{(m)}$. For convenience sake, instead of writing that p'_{ijk} ($k = 1, K$) are the discrete version of continuous functions $p' \in H^{(m)}$, we will write that the discrete functions p'_{ijk} ($k = 1, K$) belong to $H^{(m)}$.

To model the noise affecting the projections, an additive statistical model, namely the fixed-effect model (Caussinus 1986), is used. This model assumes that:

- (a) The K -vectors p'_{ij} are defined on a probability space and can be written

$$p'_{ij} = \hat{p}_{ij} + \epsilon_{ij}$$

where \hat{p}_{ij} is the non-random part (or fixed part) of p'_{ij} and ϵ_{ij} is a random error which does not depend on \hat{p}_{ij} . In this model, \hat{p} represents the reduced-noise or filtered projections one wishes to estimate.

(b) The variance of p'_{ij} can be written

$$\text{Var}[p'_{ij}] = \frac{1}{S \times N} \Gamma$$

where Γ is a (K, K) symmetric positive definite matrix.

(c) There is a Q -dimensional subspace $H_Q^{(m)}$ of $H^{(m)}$ ($Q < K$) such that all \hat{p}_{ij} belong to $H_Q^{(m)}$.

The model therefore assumes that the filtered projections belong to a subspace of the projection space which the acquired projections belong to.

3.1.2. Estimating the filtered projections. To estimate the filtered projections using the statistical model, the transform T and the subspace $H_Q^{(m)}$ must be determined. The filtered data are then obtained by projecting the transformed projections onto the subspace $H_Q^{(m)}$.

The transform T depends on the noise distribution of the acquired data. In SPECT, noise is Poisson distributed. The nonlinear transform $T(p) = \sqrt{p + 3/8}$ changes a Poisson variable into an asymptotic Gaussian variable with the following asymptotic variance (Rao 1962):

$$\Gamma = \frac{1}{4} \text{Id}$$

where Id is the (K, K) identity matrix, thus ensuring that $\text{Var}[p'_{ij}]$ does not depend on the projection angle.

$H_Q^{(m)}$ is estimated by minimizing the expression

$$\mathcal{I} = E \left[\sum_{j=1}^S \sum_{i \in I_j} \| p_{ij}^\gamma - \hat{p}_{ij} \|^2_{\Gamma^{-1}} \right] \quad (2)$$

where $E[\cdot]$ denotes the expectation, $p_{ij}^\gamma \in H_Q^{(m)}$ is the smoothed version of p'_{ij} and I_j is the set of projections i for the slice j (i.e. the sinogram corresponding to slice j). p_{ij}^γ is obtained by solving a minimization problem to approximate each projection along the direction k by a smoothing spline function of degree $2m - 1$ (appendix B). The trade-off between the fidelity to the data p'_{ij} and the smoothness of the function p_{ij}^γ is controlled by the smoothing parameter $\gamma > 0$. A single parameter γ is used for all slices.

The criterion \mathcal{I} (equation (2)) is a generalization of the criterion proposed by (Besse 1988) and previously used for filtering a single sinogram in Pélégri *et al* (1998). When filtering the projections of a volumetric distribution of activity, the criterion \mathcal{I} takes into account simultaneously the sinograms corresponding to all slices.

The solution of the minimization problem given by equation (2) is obtained using a Principal Component Analysis of smoothing spline functions involving the eigendecomposition of the matrix $W\Gamma^{-1}$, where $W = \frac{1}{S \times N} P^\gamma{}^t P^\gamma$ is the covariance matrix of the p_{ijk}^γ . t denotes the transpose, P^γ is the $(S \times N, K)$ matrix whose elements are $p_{ijk}^\gamma - \bar{p}_{jk}^\gamma$, and \bar{p}_{jk}^γ is a local centre of gravity corresponding to the mean calculated over all the projection angles i , for each bin k and each slice j .

This eigendecomposition corresponds to an eigendecomposition of the within-group variance (i.e. the variance which is not due to differences between the means of the sinograms (Benali and Escofier 1989)), where the data are discretized spline functions. The subspace $H_Q^{(m)}$ is spanned by the first Q eigenvectors associated with the largest Q eigenvalues of the

Table 2. Noise filtering algorithm.

Nonlinear transform	$p' = T(p) \implies \Gamma = \frac{1}{4}\text{Id}$
Determination of $H_Q^{(m)}$	Spline smoothing: $p' \implies p^\gamma$ Eigendecomposition of $W\Gamma^{-1}$ Projection of p^γ onto the subspace $H_Q^{(m)} \implies \hat{p}^\gamma$
Inverse nonlinear transform	$\tilde{p} = T^{-1}(\hat{p}^\gamma)$

matrix $W\Gamma^{-1}$. The filtered projections \tilde{p}_{ij} are obtained by projecting p_{ij}^γ onto $H_Q^{(m)}$ and by performing the inverse transform T^{-1} . The noise filtering algorithm is summarized in table 2.

3.2. Regularization of the estimation steps

3.2.1. Regularity properties of the first residual r^0 . Using the filtered projections \tilde{p} , the first residual r^0 can be calculated, using an FBP-type algorithm, the spline-filtered backprojection (SFBP) (Guédon and Bizais 1994, Pélégriini et al 1998).

As described in Pélégriini et al (1998) and appendix C, SFBP includes a ramp filter regularized by the Radon transform of spline kernels of degree $2m - 2$, i.e. spline kernels belonging to $H^{(m-\frac{1}{2})}$. This operator satisfies the ‘space correspondence theorem’ (Louis 1980, Natterer 1986), according to which the inverse Radon transform is continuous between Sobolev spaces. Indeed, this theorem states that if \tilde{p} is the discretization of projections of $H^{(m)}$ (modelled using spline functions of order $2m - 1$), then r^0 is the discretization of an activity distribution belonging to the Sobolev space $H^{(m-\frac{1}{2})}$ (Louis 1980); reciprocally, the projections of an activity distribution which is the discretization of a function belonging to $H^{(m-\frac{1}{2})}$ can be interpreted as the discretization of continuous projections belonging to $H^{(m)}$ (Louis 1980, Natterer 1986).

SFBP reconstruction is 2D: each slice is reconstructed independently. To ensure shift-invariance of the reconstruction process, fine projection sampling compared to the image pixel size is required (Guédon and Bizais 1994). We oversample the projections \tilde{p} by a factor $\Delta = 4$. This oversampling, performed using interpolating spline functions of order $2m - 1$, ensures that the oversampled projections still belong to $H^{(m)}$. In the following, R_{SFBP} denotes the reconstruction process which includes:

- (a) Oversampling of the projections using interpolating spline functions of order $2m - 1$.
- (b) Reconstructing an activity distribution belonging to $H^{(m-\frac{1}{2})}$ in the original spatial sampling (i.e. no oversampling of the reconstructed activity distribution).

By choosing $f^0 = 0$ (which is a particular function of $H^{(m-\frac{1}{2})}$), the first residual r^0 is the activity distribution reconstructed from the filtered projections \tilde{p} using SFBP. Incidentally, r^0 is the activity distribution reconstructed from the *acquired* projections using the regularized backprojection (RBP) described in Pélégriini et al (1998). The residual $r^0 = R_{\text{SFBP}}\tilde{p} = \text{RBP}p$ and the first direction $d^0 = r^0$ (see table 1) belong to $H^{(m-\frac{1}{2})}$. Consequently, from table 1, the operator R^* for this initialization step is RBP.

3.2.2. Regularity properties of the operator A . To ensure that the activity distributions estimated during the iterative process belong to $H^{(m-\frac{1}{2})}$, as does r^0 , it is necessary to define an operator $A = R^*R_\mu$ which ensures that the projection/backprojection of an activity distribution

belonging to $H^{(m-\frac{1}{2})}$ also belongs to $H^{(m-\frac{1}{2})}$. The attenuation distribution required to define R_μ is assumed to be known (for instance from a transmission acquisition (King *et al* 1995)).

Let g be an activity distribution belonging to $H^{(m-\frac{1}{2})}$. As R_μ is a continuous operator, the attenuated projections of g are regular and belong to $H^{(m)}$ (from the space correspondence theorem). We have shown in section 3.2.1 that R_{SFBP} ensures that the reconstruction of projections belonging to $H^{(m)}$ belongs to $H^{(m-\frac{1}{2})}$. Choosing R_{SFBP} as R^* , the oversampling process ensures that the attenuated projections $R_\mu g$ belong to $H^{(m)}$ and that the reconstructed activity distribution $R_{\text{SFBP}}R_\mu g$ belongs to $H^{(m-\frac{1}{2})}$. Therefore, the operator A defined as $R_{\text{SFBP}}R_\mu$ verifies:

$$\text{for any } g \in H^{(m-\frac{1}{2})} \Rightarrow Ag \in H^{(m-\frac{1}{2})}. \quad (3)$$

As a consequence, since $d^0 = r^0$ belongs to $H^{(m-\frac{1}{2})}$ (section 3.2.1), the reconstructed distribution t^0 belongs to $H^{(m-\frac{1}{2})}$.

3.2.3. Regularity properties of the estimated activity distributions f^n . We showed in sections 3.2.1 and 3.2.2 that f^0, r^0, d^0 and t^0 belong to $H^{(m-\frac{1}{2})}$. We now show by induction on n that the estimated activity distributions f^n also belong to $H^{(m-\frac{1}{2})}$.

Suppose that f^n, r^n, d^n and t^n belong to $H^{(m-\frac{1}{2})}$. The proof consists in verifying that $f^{n+1}, r^{n+1}, d^{n+1}$ and t^{n+1} belong to $H^{(m-\frac{1}{2})}$.

- Table 1 states that $f^{n+1} = f^n + \alpha^n d^n$ with α^n real; as f^n and d^n belong to $H^{(m-\frac{1}{2})}$, f^{n+1} also belongs to $H^{(m-\frac{1}{2})}$, under the properties of Hilbert spaces discussed in appendix A.
- Table 1 states that $r^{n+1} = r^n - \alpha^n t^n$. As r^n and t^n belong to $H^{(m-\frac{1}{2})}$, we can deduce as above that $r^{n+1} \in H^{(m-\frac{1}{2})}$.
- Table 1 states that $d^{n+1} = r^{n+1} + \beta^{n+1} d^n$. β^{n+1} is real, d^n belongs to $H^{(m-\frac{1}{2})}$ and we have just proven that r^{n+1} belongs to $H^{(m-\frac{1}{2})}$; consequently, $d^{n+1} \in H^{(m-\frac{1}{2})}$.
- Table 1 states that $t^{n+1} = Ar^{n+1} + \beta^{n+1} t^n$. β^{n+1} is real and t^n belongs to $H^{(m-\frac{1}{2})}$. We know from (3) that Ar^{n+1} belongs to $H^{(m-\frac{1}{2})}$. Therefore $t^{n+1} \in H^{(m-\frac{1}{2})}$.

This completes the proof. The final SRMR algorithm is thus the same as that given by table 1, with $R^* = \text{RBP}$ at the initialization step, $f^0 = 0$ and $A = R_{\text{SFBP}}R_\mu$. The space correspondence theorem ensures that all calculated activity distributions f^n belong to the same space $H^{(m-\frac{1}{2})}$.

In summary, four parameters are involved in the SRMR algorithm: the projection Sobolev space order m , the smoothing parameter γ , the dimension Q of the Sobolev subspace $H_Q^{(m)}$ and the number of iterations n .

4. Materials and methods

4.1. Data simulation

4.1.1. Quantification phantom. An elliptical phantom (figure 2(a)) with homogeneous regions of various intensities (table 3) was generated using the RECLBL library (Huesman *et al* 1977). The regions were large enough to avoid partial volume effects when performing quantitative measurements in the ROIs. The corresponding attenuation map is shown in figure 2(b). The linear attenuation coefficients corresponded to physiological values for a $^{99\text{m}}\text{Tc}$ acquisition (table 3). Four identical slices (one pixel thick) were generated to simulate 3D distributions. For each slice, 128 equally spaced 1D projections along a circular 360° orbit were calculated for a parallel geometry, with 128 bins per projection, using an attenuated projector of the RECLBL library. The projector did not model scatter, but was modified to

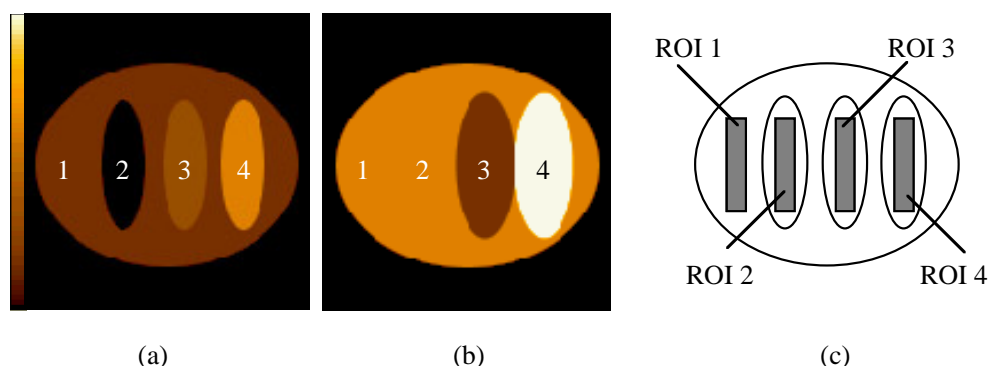


Figure 2. Quantification phantom. (a) Simulated activity distribution for each slice. (b) Corresponding attenuation map. (c) Regions of interest used for absolute quantification.

Table 3. Horizontal and vertical half-axis (L_x, L_y) (in mm), simulated activity \bar{x} (in number of events per voxel) and linear attenuation coefficients μ (in cm^{-1} , values at 140 keV) in the regions shown in figure 2(a) and figure 2(b).

Region	Activity (figure 2(a))		Attenuation (figure 2(b))	
	(L_x, L_y)	\bar{x}	(L_x, L_y)	μ
1	(248,195)	614	(248,195)	0.15 (soft tissue)
2†	(41,124)	0	—	—
3	(41,124)	1228	(56,139)	0.04 (lungs)
4	(41,124)	2456	(56,139)	0.25 (bone)

† Activity regions 1 and 2 are in the same attenuating medium.

account for a depth-dependent detector response function corresponding to that of an LEHR collimator (Formiconi *et al* 1989). The detector response was assumed to be a symmetric 1D Gaussian function with a standard deviation varying linearly with the source depth. The pixel size was 4.14 mm. Poisson noise was added to the calculated projections. The mean pixel count in each resulting sinogram was approximately 90.

4.1.2. Monte Carlo cardiac simulation. An anthropomorphic Data Spectrum cardiac phantom consisting of a left ventricle (LV) (10 mm thick wall), two lungs, a spine and a liver was considered; a $^{99\text{m}}\text{Tc}$ activity of $0.078 \text{ MBq ml}^{-1}$ (respectively $0.047 \text{ MBq ml}^{-1}$) was simulated in the LV wall (respectively in the liver). The long and short axes of the elliptical container simulating the torso were 32 and 24 cm long respectively. Narrow-beam attenuation coefficients corresponding to different compartments (soft tissue, lungs, spine and LV) and computed for any energy between 50 and 200 keV were considered.

A Monte Carlo simulation using SimSET (Harrison 1993) was performed. An LEHR collimator was modelled. Two sets of 128 2D projections each were simulated over 360° for a parallel geometry, with 128 bins and 44 slices per projection (radius of rotation of the detector 20 cm, pixel size 3.8 mm, slice thickness 5 mm). The first set contained only primary photons, i.e. attenuation was taken into account but scattered photons were discarded; the mean number of counts in the LV for a lateral projection was approximately 10. The second set consisted of ‘interaction-free’ projections (i.e. no attenuating medium was considered) and was used as a reference; the mean number of counts in the LV for a lateral projection was approximately 120. The two sets differed only in the modelling of attenuation.

4.2. Data analysis

4.2.1. Image reconstruction. All the projections of either the quantification phantom or the cardiac phantom were processed simultaneously. The depth-dependent variations of the point spread function of the detector were not compensated for.

When using MR for reconstruction, the operator R^* was FBP as in Wallis and Miller (1993). A Hann filter (cut-off frequency 0.5 pixel^{-1}) was used to reduce the effect of noise when computing the first residual r^0 (initialization step), as in La *et al* (1996) and La and Grangeat (1998). For estimation steps n , only a ramp filter (cut-off frequency 0.5 pixel^{-1}) was used.

When using SRMR for reconstruction, the parameters given in table 4 were considered. Cubic spline functions were used to model the regularity of the projections (i.e. $m = 2$). To be consistent with the space correspondence theorem, the ramp filter used in SFBP was regularized using the Radon transform of quadratic spline kernels (appendix C). One hundred iterations were performed to study the stability of the MR and the SRMR algorithms.

The interaction-free projections of the cardiac phantom were reconstructed using FBP with a ramp filter (cut-off frequency 0.5 pixel^{-1}).

Table 4. R^* operators for the SRMR algorithm.

	Quantification phantom	Cardiac phantom
Initialization	RBP ($\gamma = 10^{-4}$, $Q = 40$)	RBP ($\gamma = 0.005$, $Q = 30$)
Step n	R_{SFBP}	R_{SFBP}

4.2.2. Analysis of the reconstructed data. In the quantification phantom, the average number of counts per pixel (\bar{x}) and the corresponding standard deviation (σ) were calculated in the four rectangular ROIs (7×34 pixels each) with intrinsic uniform count density shown in figure 2(c).

In the cardiac phantom, three-dimensional ROIs were drawn in the LV wall (3093 pixel ROI) and in the liver (11692 pixel ROI). The average number of counts per pixel (\bar{x}) and the corresponding standard deviation (σ) were calculated in each ROI for the 3D activity distributions obtained (a) when reconstructing the interaction-free projections using FBP and (b) when reconstructing the attenuated projections using MR and SRMR.

5. Results

5.1. Quantification phantom

Only results regarding the first slice are presented. Similar results were obtained with the other slices.

Figures 3 and 4 show \bar{x} and $|\sigma/\bar{x}|$ respectively as a function of the iteration number n . Figure 3 demonstrates that, from iteration 25, the mean activity remained unchanged in all regions when using SRMR, while it kept increasing in ROI 2 (cold soft-tissue region) when using MR. When the mean values were stable in the hot regions, i.e. after at most 25 iterations, the relative errors between the measured and the theoretical activities were less than 5%. Figure 4 shows that $|\sigma/\bar{x}|$ also remained stable after about 25 iterations, which demonstrates the stabilization in variance of the iterative algorithm. On the other hand, $|\sigma/\bar{x}|$ diverged dramatically in all ROIs (typically after 35 iterations) with MR: between $n = 35$ and $n = 100$, $|\sigma/\bar{x}|$ increased by 15% in ROIs 3 and 4, and by more than 120% in ROIs 1 and 2.

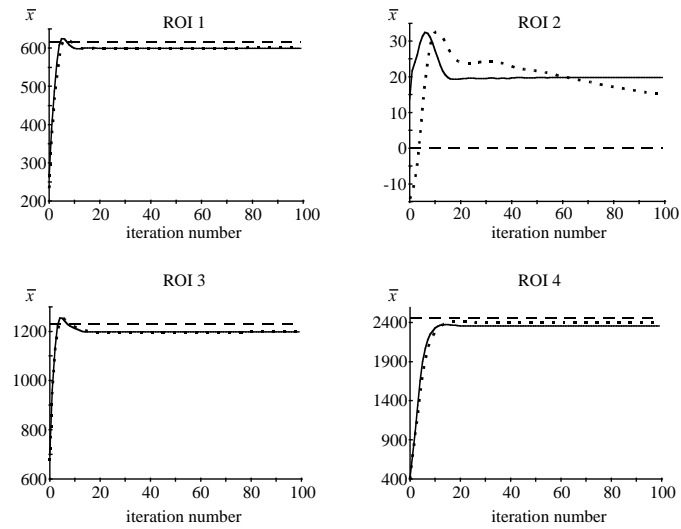


Figure 3. Quantification phantom. Plot of \bar{x} value measured in each ROI as a function of the iteration number: ---, simulated value; ·····, MR algorithm; —, SRMR algorithm.

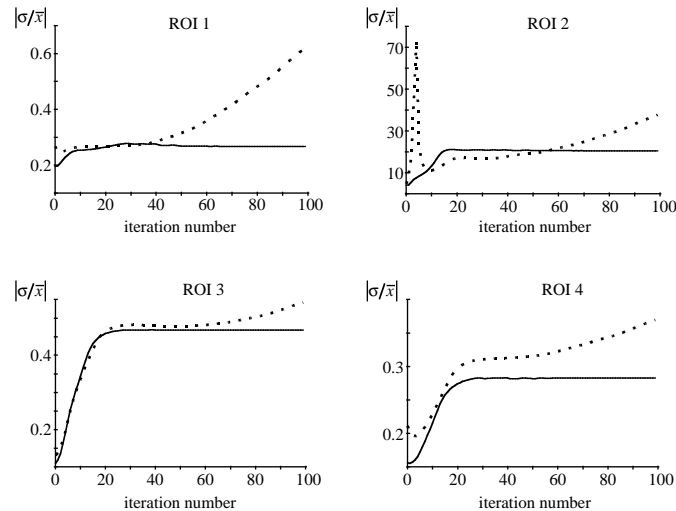


Figure 4. Quantification phantom. Plot of $|\sigma/\bar{x}|$ value measured in each ROI as a function of the iteration number: ·····, MR algorithm —, SRMR algorithm.

Figure 5 shows a reconstructed slice obtained with MR and SRMR for $n = 0$, $n = 30$ and $n = 80$, compared with the simulated slice. From table 1, the reconstructed slices f^1 obtained using MR (respectively SRMR) and $n = 0$ are proportional to the first residual r^0 obtained using FBP (respectively RBP) at the initialization step. With MR, a high-frequency noise pattern made the images obtained at iterations $n = 30$ and $n = 80$ different. On the other hand, the slices obtained using SRMR for $n = 30$ and $n = 80$ appeared identical.

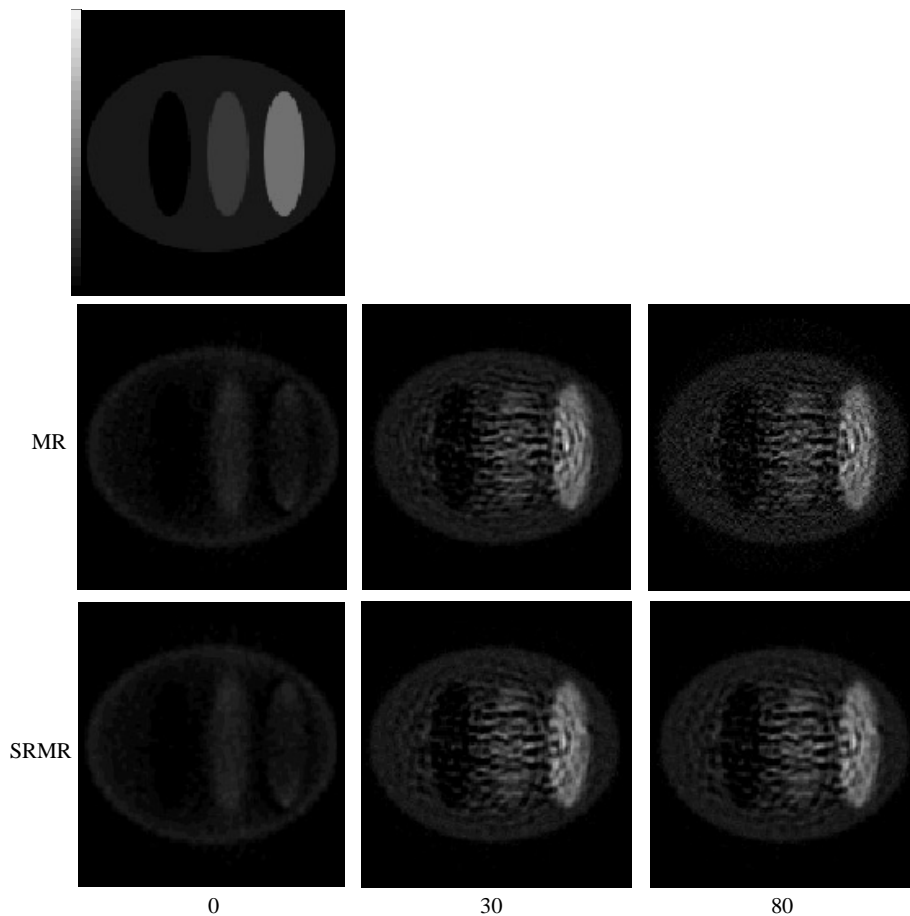


Figure 5. Quantification phantom. Top row: simulated slice. Middle row: reconstructed slice obtained with the MR algorithm. From left to right: $n = 0$, $n = 30$, $n = 80$. Bottom row: reconstructed slice obtained with the SRMR algorithm. From left to right: $n = 0$, $n = 30$, $n = 80$. The images are displayed with the same minimum and maximum values.

5.2. Cardiac phantom

Figure 6 shows \bar{x} and $|\sigma/\bar{x}|$ measured in the LV wall and in the liver respectively as a function of the iteration number n . A satisfactory convergence of the mean activity was observed with both MR and SRMR. When convergence was reached, i.e. after at most 25 iterations, the relative error between the activity measured with MR or SRMR and the activity measured in the reconstructions of the interaction-free projections was less than 1%. In the LV wall, which was affected by partial volume effect and depth-dependent blurring, the simulated activity was underestimated by about 35% with all reconstruction methods. The simulated activity in the liver (which was almost not affected by partial volume effect) was underestimated by 4% on average.

Figure 6 also demonstrates that $|\sigma/\bar{x}|$ was stable when using SRMR, after at most 25 iterations, but diverged in both the LV and the liver when using MR, after 40 iterations: between $n = 40$ and $n = 100$, $|\sigma/\bar{x}|$ increased by 7% in the LV and by more than 20% in the liver.

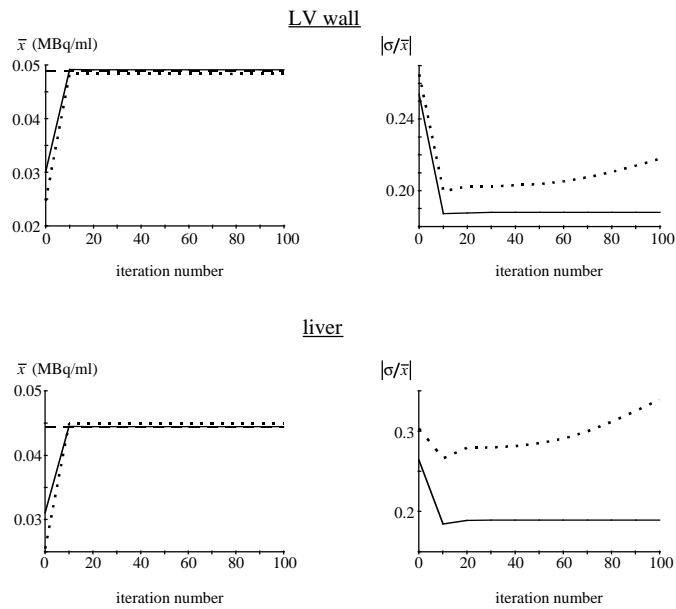


Figure 6. Cardiac phantom. Plot of \bar{x} and $|\sigma/\bar{x}|$ values measured in the LV wall and in the liver as a function of the iteration number: ---, reconstruction of interaction-free projections; ·····, MR algorithm; —, SRMR algorithm.

Figure 7 shows a transverse LV slice obtained with MR and SRMR for $n = 0$, $n = 30$ and $n = 80$, compared with the simulated slice. The reconstructed slices obtained using MR (respectively SRMR) and $n = 0$ are proportional to that obtained using FBP (respectively RBP) at the initialization step. Again, the slices obtained using SRMR for $n = 30$ and $n = 80$ were visually identical.

6. Discussion

6.1. Regularization of the MR algorithm

Iterative algorithms are the techniques of choice for non-uniform attenuation correction in SPECT, but need to be regularized to avoid divergence. The regularization approach we propose deals with both the acquisition noise and the ill-posed nature of the inversion of the Radon transform.

6.1.1. Noise filtering. The proposed method first filters the acquisition noise using the fixed-effect model, which describes the projections as a linear combination of a reduced-noise component and an error. The only assumptions are that the first and second-order moments of this error are known and that its covariance does not depend on the projections. The fixed-effect model can be used provided the covariance matrix Γ is known. This is achieved by performing a transform T on the projections. For example, $T = \text{Id}$ (identity matrix) for Gaussian distributed data (thus $\Gamma = \text{Id}$ (Anderson 1984, Benali *et al* 1994)) and $T(p) = \sqrt{p+3/8}$ for Poisson distributed data (thus $\Gamma = \frac{1}{4}\text{Id}$ (Caussinus 1986)). The filtering method can therefore be used either for original SPECT projections where noise is Poisson distributed, or for any preprocessed set of projections in which noise would be Gaussian.

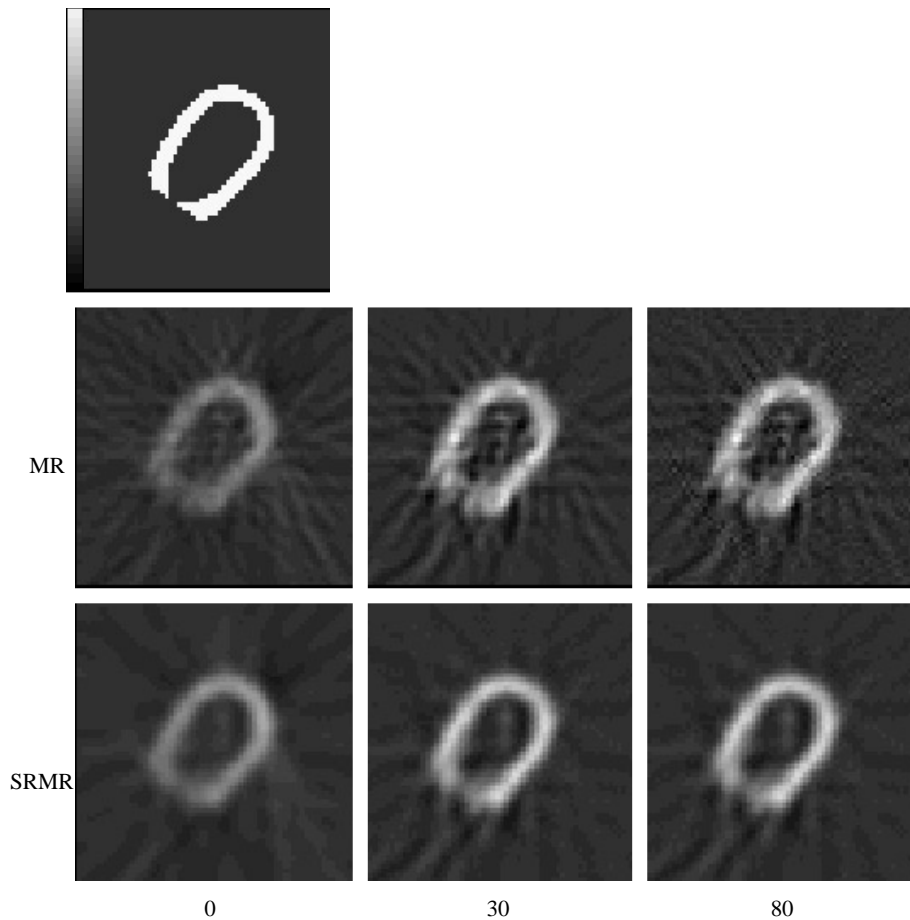


Figure 7. Cardiac phantom. Top row: simulated activated distribution for a transverse slice. Middle row: reconstructed slice obtained with the MR algorithm. From left to right: $n = 0$, $n = 30$, $n = 80$. Bottom row: reconstructed slice obtained with the SRMR algorithm. From left to right: $n = 0$, $n = 30$, $n = 80$. The images are displayed with the same minimum and maximum values.

In the absence of noise, the projections should be regular along the direction of the bins k and along the direction of the slices j . Only the regularity along the direction of the bins k is currently modelled and modelling regularity along the direction of the slices still needs to be incorporated. Moreover, the projections i are not physically independent in that sense that each projection is just a different view of the attenuated activity distribution. Future work on the fixed-effect model should take these additional properties of SPECT projections into account.

6.1.2. Regularization of the estimation steps. The regularization of the iterative procedure is performed by choosing an appropriate operator R^* for the MR algorithm.

The basic idea for using a R^* operator is to accelerate convergence by improving the numerical conditioning of the equations without altering the solution (Golub and Van Loan 1984), which corresponds to preconditioning. Several preconditioning operators have been

proposed for the conjugate gradient algorithm and applied in PET (Chinn and Huang 1997) and SPECT reconstruction (Lalush and Tsui 1994, 1995). In addition to preconditioning, regularization is also required at each iteration to avoid noise amplification. An original feature of our approach is that, in the iterative procedure, a single operator is used for both preconditioning and regularizing. The role of this operator is not only to accelerate convergence compared to the conventional conjugate gradient algorithm, but more importantly to avoid the algorithm divergence, by ensuring that all reconstructed activity distributions belong to a specific Sobolev space.

It has been shown that the operators used in the iterative filtered backprojections (Walters *et al* 1981) are good candidates for the R^* operator when using the minimal residual algorithm (La *et al* 1996, La and Grangeat 1998), but they do not ensure regularization. A spatially adaptative filtering technique has already been proposed for the regularization of MR (La *et al* 1996, La and Grangeat 1998) and applied to brain (Almeida *et al* 1997) and cardiac (La and Grangeat 1998) SPECT reconstruction: each estimated activity reconstruction is convolved with a 3D Laplacian kernel and then multiplied by a regularization parameter λ , which differs from one region to another, thus requiring a preliminary segmentation of the images.

The R^* operator used for the initialization step of the SRMR algorithm is the regularized backprojection. It ensures that the acquisition noise is filtered, and in that respect the proposed noise filtering procedure is analogous to the apodized ramp filter when FBP is used for initialization (as in MR, where a Hann filter is used for the first reconstruction). Another approach (Fessler 1993) involved a similar spline smoothing procedure along the k direction (with variable γ to deal with artefacts in the data) but the data were reconstructed using conventional FBP (with a ramp filter), which did not address the ill-posed nature of the reconstruction problem. In our approach, RBP ensures that the reconstruction problem is well-posed (from the space correspondence theorem) and that the first reconstructed activity distribution (i.e. the first residual) belongs to the Sobolev space $H^{(m-\frac{1}{2})}$, provided f^0 is an activity distribution belonging to $H^{(m-\frac{1}{2})}$. Constraining functions (here projections *and* activity distributions) to belong to a Sobolev space is equivalent to regularizing these functions by solving an optimization problem involving constraints pertaining to the derivatives of the functions (e.g. appendix B, equation (B.1)). The R^* operator used in the further estimation steps is SFBP. This ensures that all estimated distributions belong to $H^{(m-\frac{1}{2})}$.

While the initialization step uses the statistical properties of the noise affecting the projections, only continuity and derivability properties are taken advantage of in the estimation steps. It should be emphasized that, unlike in the ML-EM approaches, only the statistical properties of the *acquired* data are taken into account.

6.1.3. Parameters involved in the SRMR algorithm. SRMR involves four parameters. The order of the projection Sobolev space was $m = 2$ as in our previous work (Péligrini *et al* 1998), since cubic smoothing splines are easily calculated. Our results show that the choice of the number of iterations is not a major problem since stability was reached after at most 25 iterations for the types of data we considered.

Two parameters therefore remain to be determined: (a) the smoothing parameter γ used when fitting the projections using spline functions and (b) the dimension Q of the Sobolev subspace containing the filtered projections. Determining the appropriate combination of $[\gamma, Q]$ for removing noise without losing any relevant information is a challenge similar to determining a filter cut-off frequency and/or order. These parameters are currently chosen experimentally based upon the conclusions of our previous work (Péligrini *et al* 1998).

Experimental results on the quantification phantom (not shown) suggest that the appropriate $[\gamma, Q]$ combination only depends on the signal-to-noise ratio in the acquired projections and does not depend on the nature of the attenuating medium. For instance, the same combination $[\gamma = 10^{-4}, Q = 40]$ gave satisfactory results in air and in the case of a uniform or non-uniform attenuating medium, provided the mean number of counts in the projections was approximately 100.

6.2. Results

The SRMR approach was first validated using analytically simulated projections of a quantification phantom. These were not realistic two-dimensional projections since the attenuated sinograms were calculated independently for each slice and then stacked up. The rationale was only to study the convergence properties of SRMR.

The quantification phantom included various ‘activity/attenuation’ combinations and showed that MR diverged in terms of restored mean activity for one of these combinations (ROI 2), whereas SRMR gave stable results in all regions. We did not investigate in detail in this paper whether the divergence of MR was due to the activity distribution or to the density distribution, or to a combination of both. However, for a uniform soft-tissue medium with the same activity distribution (results not shown), the same divergence of MR was observed while SRMR gave stable results after 25 iterations at most for all regions. When using MR, the regional signal variance also kept increasing with the number of iterations, while it became stable after 25 iterations at most with SRMR.

We also studied SRMR using Monte Carlo simulations. We processed only primary projections to avoid the problem of scatter, which was beyond the scope of this work. Although the phenomena we considered (noise, attenuation and depth-dependent blurring) could be analytically simulated, Monte Carlo simulation remained more precise than analytical simulations to account for the variation of the narrow-beam attenuation coefficients with energy.

Using the Monte Carlo data, we compared the activity distributions obtained with MR or SRMR to the FBP reconstructions of interaction-free projections of the same phantom. The latter represented the ‘best’ result that could be achieved when compensating for attenuation, all other simulation parameters being identical. The resulting underestimation of the actual simulated activity, especially in the LV wall, showed the need of depth-dependent blurring and partial volume effect corrections for accurate quantitation.

Our results demonstrated that MR gave stable results in terms of restored activity but dramatically diverged in variance, making it difficult to choose an appropriate number of iterations. On the other hand, SRMR gave stable results in both mean and variance, after at most 25 iterations. As stable results were observed after at most 25 iterations for both phantoms, the convergence rate might be independent of the ‘activity/attenuation’ distribution. Although SRMR does not theoretically converge necessarily to a global minimum, constraining the reconstructed activity distributions to belong to a Sobolev space ensures the practical convergence of the mean and the variance in homogeneous regions.

All presented results regard data obtained for a 360° orbit. For the cardiac simulation, using a 360° orbit instead of a 180° orbit reduced the geometrical distortions due to the depth-dependent blurring, which was not compensated for in this paper. However, reconstruction of 180° cardiac data using SRMR has already been investigated (Péligrini 1997) and satisfactory results have been obtained.

Implementation of SRMR has not been optimized yet, leading to a computation time four times higher than with MR (10 min per iteration for the cardiac phantom on a Silicon Graphics O2 workstation). This is mainly due to the projection oversampling and to the 2D SFBP

reconstruction used in SRMR. Future work will address the optimization of spline calculations (e.g. using methods described in Unser *et al* (1993)) and the use of a fully 3D reconstruction algorithm to complete the filtering procedure proposed in this paper.

7. Conclusion

To address the problem of measurement noise and computational noise, which contributes to the ill-posed nature of the reconstruction problem in the presence of attenuation, we proposed a new spline-based regularization method for the minimal residual algorithm, called SRMR. SRMR uses the space correspondence theorem which states that the inverse Radon transform is continuous between Sobolev spaces, i.e. that the reconstructed activity distributions have specific continuity and derivability properties which can be deduced from those of their projections. We first take advantage of the intrinsic regularity properties of the acquired projections in solving a statistical model which reduces the Poisson measurement noise and ensures that the resulting filtered projections belong to a known Sobolev space. We then reduce computational noise during the iterative reconstruction procedure used to correct for attenuation, by using a regularized backprojection method, the SFBP. This ensures that the activity distributions estimated at each iteration belong to the Sobolev space consistent with the Sobolev space the projections belong to (from the space correspondence theorem).

Analytical and Monte Carlo simulations demonstrate that such a regularization gives stable results after at most 25 iterations. Further studies will include detailed comparison with other existing attenuation correction schemes, such as ML-EM approaches, and combination of the proposed processing approach with scatter correction and compensation for depth-dependent blurring and partial volume effects.

Acknowledgments

The authors thank an anonymous referee for helpful comments on earlier versions of this manuscript. M Péligrini and G El Fakhri thank the ‘Institut de Formation Supérieure Biomédicale’ (Villejuif, France) and Sopha Medical Vision International (Buc, France) for supporting their PhDs.

Appendix A. Sobolev spaces

This section introduces the general definition of Sobolev spaces. For more details, we refer the reader to Adams (1975) and Natterer (1986).

Let $\mathcal{S}(\mathbb{R}^n)$ denote the Schwartz space: the linear space of those infinitely differentiable functions $f(x)$ with compact support in \mathbb{R}^n , which fall to 0 faster than any power of $1/x$ as $|x|$ tends to infinity (and so do all their derivatives). Let $\mathcal{S}'(\mathbb{R}^n)$ denote the space of tempered distributions, i.e. the space of linear functionals \mathcal{F} defined over $\mathcal{S}(\mathbb{R}^n)$. The general definition of a Sobolev space of real order α , $H^{(\alpha)}$, is (Adams 1975, Natterer 1986, Triebel 1992):

$$H^{(\alpha)} = \{\mathcal{F} \in \mathcal{S}'(\mathbb{R}^n) : (1 + |\xi|^2)^{\alpha/2} \widehat{\mathcal{F}} \in \mathcal{L}_2(\mathbb{R}^n)\}$$

where $\xi \in \mathbb{R}$, $\widehat{\mathcal{F}}$ denotes the Fourier transform of \mathcal{F} and $\mathcal{L}_2(\mathbb{R}^n)$ denotes the space of functions on \mathbb{R}^n the square of which has a finite integral.

Functions \mathcal{F} are said to be ‘ α times differentiable in the sense of Sobolev’. The smoothness or ‘Sobolev regularity’ of \mathcal{F} can be measured by the number of times \mathcal{F} is differentiable (Triebel 1992).

The following results hold:

- (a) $H^{(\alpha)}$ is a Hilbert space (Natterer 1986) with norm

$$\|\mathcal{F}\|_{H^{(\alpha)}} = \left(\int_{\mathbb{R}^n} (1 + |\xi|^2)^\alpha |\widehat{\mathcal{F}}(\xi)|^2 d\xi \right)^{\frac{1}{2}}.$$

Consequently, (1) for all $\mathcal{F} \in H^{(\alpha)}$ and $a \in \mathbb{R}$, $a\mathcal{F} \in H^{(\alpha)}$ and (2) for all $\mathcal{F}_1 \in H^{(\alpha)}$ and $\mathcal{F}_2 \in H^{(\alpha)}$, $\mathcal{F}_1 + \mathcal{F}_2 \in H^{(\alpha)}$.

- (b) For $m \geq 0$ an integer, $H^{(m)}$ consists of those functions whose derivatives of order up to $m - 1$ are absolutely continuous and whose m th derivative is in $\mathcal{L}_2(\mathbb{R}^n)$ (Wahba 1990).
(c) If $\alpha > m + \frac{1}{2}$, m an integer, one can verify that \mathcal{F} is m times continuously differentiable (Triebel 1992).

Appendix B. Spline functions as solutions for smoothing problems

The so-called ‘smoothing problem’ consists in finding a function h^γ which is a smoothed approximation of a function f , assuming that h^γ has known properties of continuity and derivability. As a particular case, it may be assumed that h^γ has an absolutely continuous $(m - 1)$ th derivative and a square integrable m th derivative (Schoenberg 1964), i.e. h^γ belongs to the Sobolev space $H^{(m)}$, m an integer (appendix A). h^γ is obtained by solving the following minimization problem:

$$h^\gamma = \min_{h \in H^{(m)}} \|h - f\|_{H^{(m)}}^2 + \gamma \|h^{(m)}\|^2 \quad (\text{B.1})$$

where $\|\cdot\|_{H^{(m)}}$ is the norm defined on $H^{(m)}$ (appendix A), γ is called the smoothing parameter and $h^{(m)}$ is the m th derivative of h . γ controls the trade-off between the fidelity to the data f and the smoothness of the solution (Wahba 1990, Fessler 1993).

It has been shown (Schoenberg 1964) that h^γ is a spline function of order $2m - 1$ sampled at knots k ($k = 1, K$), i.e. h^γ is piecewise polynomial of degree $2m - 1$ in each interval $[k, k + 1]$, with the pieces joined at the knots k so that h^γ has $2m - 2$ continuous derivatives. The space of spline functions of order $2m - 1$ is thus a compact subspace of $H^{(m)}$.

Appendix C. Space correspondence theorem and discrete reconstruction schemes

This section briefly describes how a discrete reconstruction problem may be solved using the theory of Sobolev spaces. This requires (1) interpreting discrete activity distributions as the discretization of functions belonging to a Sobolev space and (2) designing a reconstruction algorithm which satisfies the space correspondence theorem. For more details, we refer the reader to Ohya *et al* (1987) and Guédon and Bizais (1991, 1994).

Appendix C.1. Discrete activity distributions

Discretizing a function $f(x, y)$ (e.g. a 2D distribution of activity) on a grid with pixel size d consists in applying a prefilter $g(x, y)$ (e.g. an anti-aliasing filter such as the ideal low-pass filter of the Shannon sampling theorem) to $f(x, y)$ and sampling thereafter, i.e. taking the values of the prefiltered function at points $l = xd, l' = yd$:

$$f_{ll'} = g(x, y) * * f(x, y)|_{x=l/d, y=l'/d} \quad (\text{C.1})$$

where $**$ denotes a 2D convolution operator. The space the activity distribution belongs to is entirely determined by the nature of the prefilter g . If $g \in H^{(\alpha)}(\mathbb{R}^2)$, $g * * f \in H^{(\alpha)}(\mathbb{R}^2)$. $f_{ll'}$ is thus the discretization of a continuous function of $H^{(\alpha)}(\mathbb{R}^2)$.

Appendix C.2. Spline-filtered backprojection (SFBP)

The conventional FBP reconstruction of a continuous activity distribution $f(x, y)$ from its continuous projections $p(r, \theta)$ can be written as:

$$f(x, y) = \mathcal{B}\{h(r) * p(r, \theta)\} \quad (\text{C.2})$$

where \mathcal{B} denotes the backprojection operator, $*$ denotes 1D convolution along the radial direction r and $h(r)$ denotes the inverse Fourier transform of the ramp filter.

Using equation (C.2) and the central slice theorem, it can be shown that the 2D convolution of g and f (equation (C.1)) is the reconstruction of the 1D convolution of their continuous projections $p^g(r, \theta)$ and $p(r, \theta)$, hence:

$$g(x, y) * f(x, y) = \mathcal{B}\{h(r) * p^g(r, \theta) * p(r, \theta)\} = \mathcal{B}\{b(r, \theta) * p(r, \theta)\}.$$

$b(r, \theta)$ can be interpreted as an angle-dependent spline-regularized ramp filter.

SFBP consists in choosing the Radon transform of a 2D spline kernel g (i.e. a B-spline (Unser *et al* 1993, Guédon and Bizais 1991)) for p^g . For instance, $b_0(r, \theta) = h(r) * p_0^g(r, \theta)$, where $p_0^g(r, \theta)$ is the Radon transform of the 2D spline kernel of degree 0, is called the Haar filter (Guédon and Bizais 1994). In this paper, the space correspondence theorem determines the spline kernel g to be used. Since the projections are modelled in $H^{(m)}$, g must be a spline kernel belonging to $H^{(m-\frac{1}{2})}$ (a spline function of degree $2m - 2$) so that the reconstructed distribution lies in $H^{(m-\frac{1}{2})}$.

To use SFBP on discrete projections p which are the discretization of projections $p \in H^{(m)}$, we process each slice independently by:

- Oversampling the projections p_{ik} by a factor $\Delta = 4$ using interpolating splines of degree $2m - 1$.
- Computing the discrete version p_{ik}^g of p^g , using $2m - 2$ successive convolutions of the discrete version of the Haar filter by the discrete version of p_0^g , whose expressions can be found in Guédon and Bizais (1994).
- Convoluting the oversampled p_{ik} by p_{ik}^g in the k direction.
- Backprojecting the convolved projections using conventional algorithms (e.g. from Huesman *et al* (1977)). This yields a discrete activity distribution in its original sampling $f_{II'}$. From equation (C.1), $f_{II'}$ is the discrete version of an activity distribution f belonging to $H^{(m-\frac{1}{2})}$.

References

- Adams R 1975 *Sobolev Spaces* (New York: Academic)
- Almeida P, Ribeiro MJ, Bottlaender M, de Dreuille O, Loc'h C, Mazière B and Bendriem B 1997 Quantitative kinetics of 123I-Epidopride in baboon brain, measured with attenuation corrected SPECT *Eur. J. Nucl. Med.* **24** 1036
- Anderson T W 1984 The 1982 Wald Memorial Lectures. Estimating linear statistical relationships *Ann. Statist.* **12** 1–45
- Axelsson O 1980 Conjugate gradient type methods for unsymmetric and inconsistent systems of linear equations *Linear Algebra Appl.* **29** 1–16
- Bellini S, Piacentini M, Cafforio C and Rocca F 1979 Compensation of tissue absorption in emission tomography *IEEE Trans. Acoust. Speech Signal Process.* **27** 213–18
- Benali H and Escofier B 1989 Smooth factorial analysis and factorial analysis of local differences *Multivariate Data Analysis* ed R Coppi and S Bolasco (Amsterdam: Elsevier) pp 327–39
- Benali H, Guédon J P, Buvat I, Péligrini M, Bizais Y and Di Paola R 1994 A statistical model for tomographic reconstruction methods using spline functions *Proc. SPIE* **2299** 242–51
- Besse P 1988 Spline functions and optimal metric in linear principal component analysis *Component and Correspondence Analysis* ed J L A Van Rijkevorsel and J De Leeuw (London: Wiley) pp 81–103

- Caussinus H 1986 Models and uses of principal component analysis *Multidimensional Data Analysis* ed J De Leeuw (Leiden: DSWO) pp 149–70
- Chang L T 1978 A method for attenuation correction in radionuclide computed tomography *IEEE Trans. Nucl. Sci.* **25** 638–43
- Chinn G and Huang S C 1997 A general class of preconditioners for statistical iterative reconstruction of emission computed tomography *IEEE Trans. Med. Imaging* **16** 1–10
- Fessler J A 1993 Tomographic reconstruction using information-weighted spline smoothing *Information Processing in Medical Imaging* ed H H Barrett and A F Gmitro (Berlin: Springer) pp 372–86
- Formiconi A R, Pupi A and Passeri A 1989 Compensation of spatial system response in SPECT with conjugate gradient reconstruction technique *Phys. Med. Biol.* **34** 69–84
- Golub G H and Van Loan C F 1984 *Matrix Computations* (Baltimore, MD: Johns Hopkins University Press)
- Green P J 1990 Bayesian reconstructions from emission tomography data using a modified EM algorithm *IEEE Trans. Med. Imaging* **9** 84–93
- Greenbaum A 1997 *Iterative Methods for Solving Linear Systems* (Philadelphia, PA: Society for Industrial and Applied Mathematics)
- Guédon J P and Bizais Y 1991 Spline-based regularisation for discrete FBP reconstruction *Information Processing in Medical Imaging* ed A C F Colchester and D J Hawkes (Berlin: Springer) pp 59–67
- 1994 Bandlimited and Haar filtered back-projection reconstructions *IEEE Trans. Med. Imaging* **13** 430–40
- Harrison R L 1993 Preliminary experience with the photon history generator module of a public-domain simulation system for emission tomography *Conf. Rec. 1993 IEEE Nucl. Sci. Symp. Med. Imaging Conf.* **2** 1154–58
- Hudson H M and Larkin R S 1994 Accelerated image reconstruction using ordered subsets of projection data *IEEE Trans. Med. Imaging* **13** 601–9
- Huesman R H, Gullberg G T, Greenberg W L and Budinger T F 1977 RECLBL library users manual: Donner algorithms for reconstruction tomography *Lawrence Berkeley Laboratory, University of California Publication* 214
- Kawata S and Nalcioglu O 1985 Constrained iterative reconstruction by the conjugated gradient method *IEEE Trans. Med. Imaging* **4** 65–71
- King M A, Tsui B M W and Pan T S 1995 Attenuation compensation for cardiac single-photon emission computed tomographic imaging: Part 1. Impact of attenuation and methods of estimating attenuation maps *J. Nucl. Cardiol.* **2** 513–24
- King M A, Tsui B M W, Pan T S, Glick S J and Soares E J 1996 Attenuation compensation for cardiac single-photon emission computed tomography imaging: Part 2. Attenuation compensation algorithms *J. Nucl. Cardiol.* **3** 55–63
- La V and Grangeat P 1998 Minimal residual cone-beam reconstruction with attenuation correction in SPECT *Phys. Med. Biol.* **43** 715–27
- La V, Grangeat P, Iovleff S, Mallon A and Sire P 1996 The use of the least-squares minimal residual algorithm for fast and regularized attenuation compensation in SPECT *Conf. Rec. 1996 IEEE Nucl. Sci. Symp. Med. Imaging Conf.* **3** 1658–62
- Lalush D S and Tsui B M W 1994 Improving the convergence of iterative filtered backprojection algorithms *Med. Phys.* **21** 1283–86
- 1995 A fast and stable maximum *a posteriori* conjugate gradient reconstruction algorithm *Med. Phys.* **22** 1273–84
- Louis A K 1980 Approximation of the Radon transform from samples in limited range *Mathematical Aspects of Computerized Tomography* ed G T Herman and F Natterer (Berlin: Springer) pp 127–39
- Murase K, Itoh H, Mogami H, Ishine M, Kawamura W, Iio A and Hamamoto K 1987 A comparative study of attenuation correction algorithms in single photon emission computed tomography (SPECT) *Eur. J. Nucl. Med.* **13** 55–62
- Natterer F 1986 *The Mathematics of Computerized Tomography* (Stuttgart: Wiley)
- Ohyama N, Ohki S, Inoue S, Tsujiuchi J and Honda T 1987 Discrete Radon transform in a continuous space *J. Opt. Soc. Am. A* **4** 318–24
- Pélégrini M 1997 Quantification en tomographie d'émission monophotonique—Méthodologie globale pour la reconstruction et la correction de phénomènes physiques *PhD Dissertation* Université Paris XI Orsay, France
- Pélégrini M, Benali H, Buvat I, El Fakhri G and Di Paola R 1998 Two-dimensional statistical model for regularized backprojection in SPECT *Phys. Med. Biol.* **43** 421–34
- Rao C R 1962 *Linear Statistical Inference and its Applications* (New York: Wiley) pp 357–8
- Schoenberg I 1964 Spline functions and the problem of graduation *Proc. Natl. Acad. Sci. USA* **52** 947–50
- Tretiak O and Metz C 1980 The exponential Radon transform *SIAM J. Appl. Math.* **39** 341–54
- Triebel H 1992 *Theory of Function Spaces* (Boston, MA: Birkhäuser)
- Unser M, Aldroubi A and Eden M 1993 B-spline signal processing: Part II - Efficient design and applications *IEEE Trans. Signal Processing* **41** 834–48
- Wahba G 1990 *Spline Models for Observational Data* (Philadelphia, PA: Society for Industrial and Applied Mathematics)

- Wallis J W and Miller T R 1993 Rapidly converging iterative reconstruction algorithms in single photon emission computed tomography *J. Nucl. Med.* **34** 1793–800
- Walters T E, Simon W, Chesler D A and Correia J A 1981 Attenuation correction in gamma emission computed tomography *J. Comput. Assist. Tomogr.* **5** 89–94
- Zhao X D, Tsui B M W, Gregoriou G K, Lalush D S, Li J and Eisner R L 1994 Evaluation of corrective reconstruction methods using a 3D cardiac-torso phantom and bull's eye plots *IEEE Trans. Nucl. Sci.* **41** 2831–7